In Situ Observation of Cirrus Scattering Phase Functions with 22° and 46° Halos: Cloud Field Study on 19 February 1998

FREDERIQUE AURIOL, JEAN-FRANÇOIS GAYET, GUY FEBVRE, AND OLIVIER JOURDAN

Laboratoire de Météorologie Physique, UMR/CNRS N°6016, Université Blaise Pascal, Clermont-Fd, France

LAURENT LABONNOTE AND GERARD BROGNIEZ

Laboratoire d'Optique Atmosphérique, UMR/CNRS N°8518, Université des Sciences et Techniques de Lille, Lille, France

(Manuscript received 26 September 2000, in final form 6 February 2001)

ABSTRACT

Observations of halos and related phenomena due to ice crystals are commonly reported from ground observations and presented in the literature. Nevertheless, ice crystal characteristics have only been poorly documented from in situ measurements performed in halo-producing cirrus with simultaneous observations of optical phenomena. Using the Polar Nephelometer, a new instrument for in situ measuring of the scattering phase function of cloud droplets and ice particles, 22° and 46° halo features have been evidenced during a cirrus uncinus cloud case study between −30°C and −38°C. Simultaneous microphysical measurements were made with a 2D-C probe manufactured by Particle Measuring Systems Inc. (PMS). The results show that ice crystal properties derived from 2D-C measurements do not present substantial differences when comparing cirrus cloud samples with and without halos. Consequently, the cloud scattering properties appear to be dominated by small ice particles (smaller than about 100 μm), which are poorly documented with conventional PMS probes. The halo occurrences are observed in only a few cloud portions (2%), which are characterized by small horizontal scales (100–400 m). Furthermore, the observed 22° and 46° peak features are smoothed out with regard to modeling results relative to geometric pristine-crystal shape. These differences are discussed by using the new Inhomogeneous Hexagonal Monocrystal theoretical model of light scattering.

1. Introduction

In the early eighteenth century Mariotte (1717) was the first to attribute halos to prismatic ice crystals. He showed that the 22° halo is caused by randomly oriented ice crystals. Since then, observations of halos and related phenomena due to ice crystals have been frequently reported in the literature, even as recently as the finely illustrated review by Tape (1994), which displays pictures of Antarctic atmospheric halos with subsequent interpretations from ray tracing models. Theoretical studies of various optical phenomena associated with the light scattering properties of ice crystals have been subjected to considerable works these last 10 years within the critical global climate issue involving cirrus clouds. Different techniques have been used to model the scattering phase functions for crystals of different regular shapes [see among the more recent works Macke and Mishchenko (1998), Liou et al. (1999); Eide et al. (1999)]. Most of the theoretical results that consider simple geometric ice crystals show rather sharp peaks related to the well-known 22° and 46° halos. Nevertheless, the rare ground-observed occurrences of these optical phenomena indicate serious deficiencies in the theoretical approaches. Two mechanisms are involved to explain the absence of halos. The first mechanism is due to the fact that highly regular pristine ice crystals are rarely observed in cirrus clouds (Heymsfield et al. 1990; Korolev et al. 1999). In support of these findings, Francis (1995) showed that the 22° halo was absent from radiance field measurements within cirrus clouds and that first direct in situ measurements of the scattering phase function in cirrostratus clouds (Gayet et al. 1998) did not evidence 22° halos. Direct measurements of the scattering phase function in laboratories (Volkovitskiy et al. 1980; Lawson and Jensen 1998) confirmed these findings, whereas Crépel et al. (1997) did detect a very smoothed 22° peak. Ground-based aureolemeter measurements by Brogniez et al. (1995) showed a pronounced 22° halo. However, the authors also showed that the radiance field around the halo is smoother than the modeling results, relative to hexagonal ice crystals, can predict. As confirmed by recent theoretical studies (Liou et al. 1998; Yang and Liou 1998; Knap et al. 1999), the imperfect crystal geometry hampers the for-

Corresponding author address: Jean-François Gayet, LaMP, Université Blaise Pascal, 24, Av. des Landais, 63177 Aubière, France.
E-mail: gayet@opgc.univ-bpclermont.fr

mation of halo. The second mechanism addresses small ice crystals that do not generate halos. Earlier laboratory studies (Sassen and Liou 1979) and recent theoretical results (Yang and Liou 1996; Mishchenko and Macke 1999) both showed that ice crystal dimension on the order of 20 μm (at visible wavelengths) appears to delineate the lower limit of ice crystal size responsible for halo formation.

In this paper we show from an airborne case study of a cirrus uncinus cloud that measured scattering phase function does exhibit 22° and 46° halo features in few cloud portions. These optical properties are compared to subsequent ice particles characteristics, then discussed by using a new theoretical model of light scattering (Labonnote et al. 2001).

2. Aircraft instrumentation and flight location

a. Aircraft instrumentation and data processing

An instrumented TBM700 aircraft was operated during an experiment (called CIRRUS '98) devoted to study microphysical–radiation interactions in cirrus clouds. This single turbo-propeller aircraft is developed and manufactured by SOCATA Inc. in Tarbes (South-West of France). For this experiment, the operational ceiling of the aircraft was extended from 30 000 to 35 000 ft and the standard avionics was supplemented with an inertial platform, an air data unit, and a global positioning system (GPS) with time output used to synchronize the airborne measurements (Durand et al. 1998). An airborne Infrared Cryogenic Spectrometer (Durand et al. 1998) was installed onboard but the infrared spectral radiance measurements will not be discussed here as it is beyond the scope of the paper. Two in situ microphysical probes were mounted on the TBM700: a PMS 2D-C for recording the cloud particle images between 25- and 800-μm diameter and the Polar Nephelometer. The data from both the PMS 2D-C and Polar Nephelometer probes were recorded using a data acquisition system (Motorola computer) connected to a laptop PC for real-time probe operations. We recall that the Polar Nephelometer is a unique airborne in situ instrument, that is compatible with the PMS canister [for a detailed description of the Polar Nephelometer operation, see Gayet et al. (1997)]. This instrument measures the scattering phase function of an ensemble of cloud particles (i.e., water droplets ice crystals, or a mixture of these particles from a few micrometers to about 500-μm, diameter) that intersect a collimated laser beam near the focal point of a paraboloidal mirror. The light that scattered at polar angles from $\pm 3.49°$ to $\pm 169°$ is reflected onto a circular array of 44 photodiodes. The laser beam is provided by a high-power (1.0 W) multimode laser diode operating at $\lambda = 804$ nm. The data acquisition system can record the measured scattering phase functions with a sampling period that can be manually set from 10 s (0.1 Hz) to 1 ms (1 kHz). The direct measurement of the scattering phase function enables us to recognize particle types (water droplets or ice crystals), to calculate the optical parameters (extinction coefficient and asymmetry parameter), and to retrieve the cloud microphysical properties (particle size spectra, liquid water and ice contents, particle concentration) with the inversion method developed by Oshchepkov et al. (1993). The sensitivity of the Polar Nephelometer probe allows us to detect ice crystals as small as a few microns in diameter.

b. Description of the methods of data processing

Most of the processed parameters (including microphysical and thermal dynamic properties and aircraft position) were reduced to 1-Hz sampling frequency, which corresponds to a spatial resolution of about 100 m at the mean cruising speed of the TBM700.

1) METHOD OF 2D-C DATA PROCESSING

The method of 2D-C data processing used in this study and the uncertainties on the derived microphysical parameters have already been described in details in Gayet et al. (1996a). We recall that the method provides, at 1-Hz frequency, the size spectrum distributed over 32 channels (each having a 25-μm resolution from 25- to 800-μm size range) and the usual microphysical parameters: ice particle concentration (C2D), mean particle size (D2D), and ice water content (IWC). It should be noted that the TBM700 aircraft was neither equipped with a PMS 2D-P nor a PMS forward scattering spectrometer probe (FSSP). This does not introduce any error in sizing large particles because only ice particles smaller than around 500 μm were sampled during the present study. On the contrary, a large source of errors arose from the lack of measurements of small ice particles [(i.e., smaller than 50 μm; see Larsen et al. (1998)], which are usually detected in cirrus clouds (Platt et al. 1989; Heymsfield et al. 1990). Consequently, significant uncertainties are inherent to both the probe characteristics and the lack of measurements of small ice particles, but the relative fluctuations of the microphysical parameters probably reflect the actual cloud microstructure.

2) METHOD OF POLAR NEPHELOMETER DATA PROCESSING

The data reduction of the Polar Nephelometer measurements has already been described in Gayet et al. (2000). We recall that the comparison between the microphysical parameters retrieved from the Polar Nephelometer measurements (Oshchepkov et al. 1993) with those calculated from the size distribution measurements by the PMS FSSP-100 highlighted the reliability of the airborne version of the Polar Nephelometer for measuring the scattering phase function.

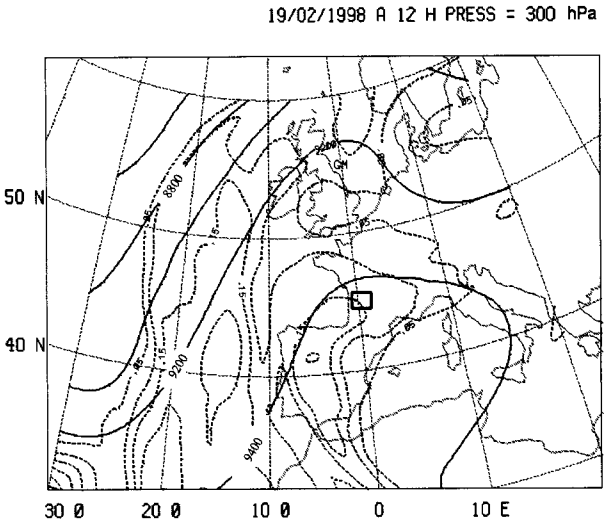

FIG. 1. The 300-hPa geopotential chart with humidity fields at 1200 UTC on 19 Feb 1998. The rectangular frame depicts the area of the cloud cirrus sampling discussed in this paper.

The extinction coefficient (σ_{ext}) is derived from the measured scattering phase function assuming randomly oriented nonabsorbing particles (Auriol 1998). In the presence of ice crystals, we may reasonably assume that the Polar Nephelometer measurement improves the extinction coefficient estimate (accuracy within 15%) with regard to PMS probe measurements because the measured phase function represents the contribution of scattering energies of either water droplets, ice crystals, or a mixture of these particles.

Because the measurements at small forward scattering angles ($\theta < 15°$) are not available due to the diffracted light pollution caused by the edges of holes that are drilled on the paraboloidal mirror (Gayet et al. 1997), the asymmetry parameter (g) has been determined according to the method of Gerber et al. (2000). This method assumes that the diffraction and refraction components of the scattered light at small scattering angles $\theta < 15°$ can be separated. The subsequent ratio f of the diffracted portion of the scattered light to the total scattered light has been determined for nonabsorbing large spheres to be $f = 0.56$ by using Mie calculations and by assuming typical measured water droplet spectra. We have assumed the value of $f = 0.56$ even for ice particles because this value is close to the average value, which can be estimated from the theoretical results of Takano and Liou (1989, 1995), obtained for a variety of ice crystal shapes. Nevertheless, significant uncertainties may remain on g-value determination due to deficiencies in theoretical approches, particularly for irregular-shaped ice crystals, but the relative fluctuations of g probably reflect the actual cloud optical properties.

c. Meteorological situation

The observations presented in this study were obtained on 19 February 1998 and the TBM700 flight

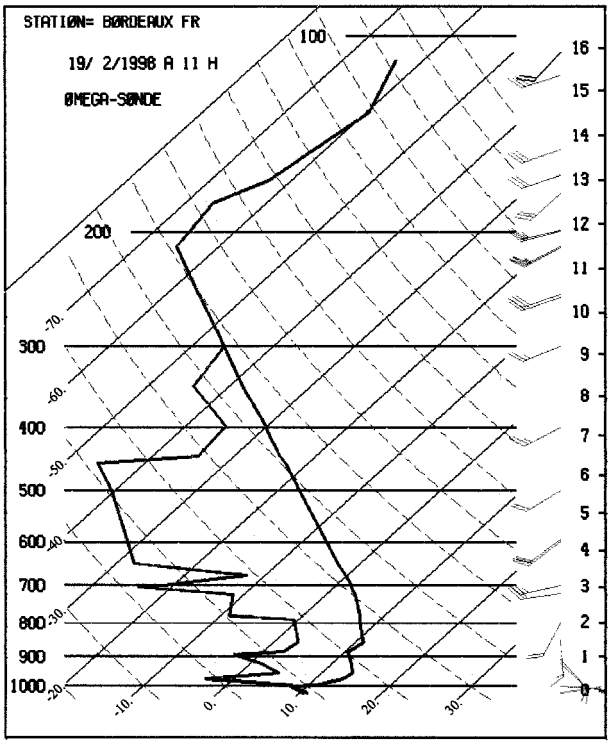

FIG. 2. Vertical sounding of the air, dewpoint temperatures, and wind obtained in Bordeaux, France, at 1100 UTC on 19 Feb 1998.

lasted from 1340 to 1700 UTC. Figure 1 represents the synoptic 300-hPa geopotentials with humidity field at 1200 UTC and the location of the experiment area (rectangular frame). The meteorological situation was characterized by a persistent high pressure system centered over France with humid air at higher troposphere levels coming over the experimental area from the southwest. The vertical sounding shown in Fig. 2 was obtained close to the experiment area (Bordeaux) at 1100 UTC. Despite well-known uncertainties on humidity measurements at high levels, the sounding shows a wet layer that roughly corresponds to the cirrus cloud detected from the aircraft, namely, between 7200 m mean sea level (MSL)/−30°C and 10 800 m MSL/−60°C. Much dryer air characterizes the lower layers. Figure 2 also indicates within the cirrus levels southwesterly (225°) wind with a speed increasing with the altitude from 14 to 18 m s^{-1}. The analysis of the *National Oceanic and Atmospheric Administration-14*–advanced very-high resolution radiometer image sampled at 1434 UTC reveals rather scattered cirrus cloud field in the experiment area and, put together with visual observations from the aircraft, the studied cirrus has been classified as cirrus uncinus.

3. Evidence of the 22° and 46° halos in cirrus uncinus clouds

Figure 3 shows the time series of microphysical and optical parameters obtained by the aircraft during a rep-

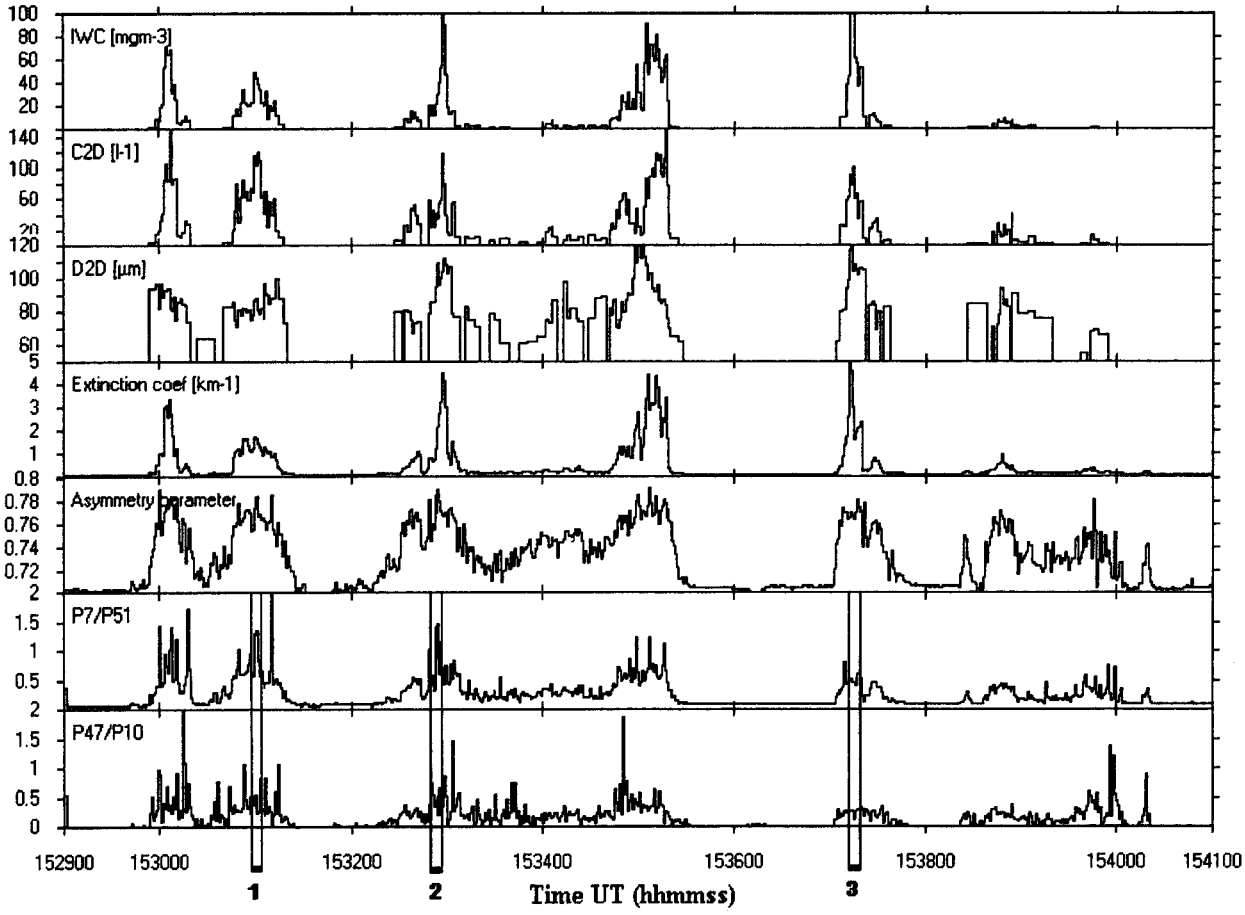

FIG. 3. Time series of the TBM700 parameters measured during the flight on 19 Feb 1998 at the 7600 m/−35°C level in cirrus uncinus clouds.

resentative 12-min sample of the cirrus at the 7600 m MSL/−35°C level. These parameters are, respectively, IWC, C2D, D2D (these three parameters being inferred from 2D-C data); the extinction coefficient (σ_{ext}) and the asymmetry parameter (g) (both inferred from the Polar Nephelometer); the ratio of the values measured by the Polar Nephelometer at the scattering angles of 22° and 18.5° (ratio of channel 7 to channel 51, P7:P51); and the ratio of the values measured at 46° and 44.5° (ratio of channel 47 to channel 10, P47:P10). As we state below, the values of the P7:P51 and the P47:P10 ratios will lead to the determination of a quantitative criteria for the occurrence of the 22° and 46° halos, respectively.

The examination of the results in Fig. 3 reveals a common feature in cirrus uncinus microphysical properties, that is to say, several cloud parts (5–10 km long) with large horizontal heterogeneities [see, among others, Gayet et al. (1996a)]. The ice water content and the ice particle concentration reach 0.1 g m^{-3} and 150 L^{-1}, respectively, and the mean size ranges from 70 to 120 μm.

According to the results of the time series in Fig. 3, we have selected three typical examples of scattering phase functions with relevant cloud microphysical charateristics. The corresponding time intervals have been reported in Fig. 3 and labeled 1–3. The first example in Fig. 4 concerns a 6-s sampling from 1530:56 where the P7:P51 values are rather high (>1.0). The upper panel of Fig. 4 represents the mean scattering phase function measured by the Polar Nephelometer (solid circles) with an arbitrary example of theoretical scattering phase function (dotted line) relative to randomly oriented hexagonal crystal plates with an aspect ratio (Q) of 0.2. The lower-left panel displays the corresponding 2D-C particle size distribution with the subsequent mean values of the relevant parameters, whereas the lower-right panel represents examples of ice particle images sampled by the 2D-C. The results show that the measured scattering phase function clearly exhibits the 22° and 46° halo features. As a matter of fact the measured value at 22° (channel 7) is significantly larger than the 18.5° one (channel 51) leading to a P7/P51 ratio of about 1.5 (see Fig. 3). As for the 46° halo, the ratio P47:P10 is only 1.1, leading to a smoothed peak at 46°.

The time series in Fig. 3 also reveal that the halo

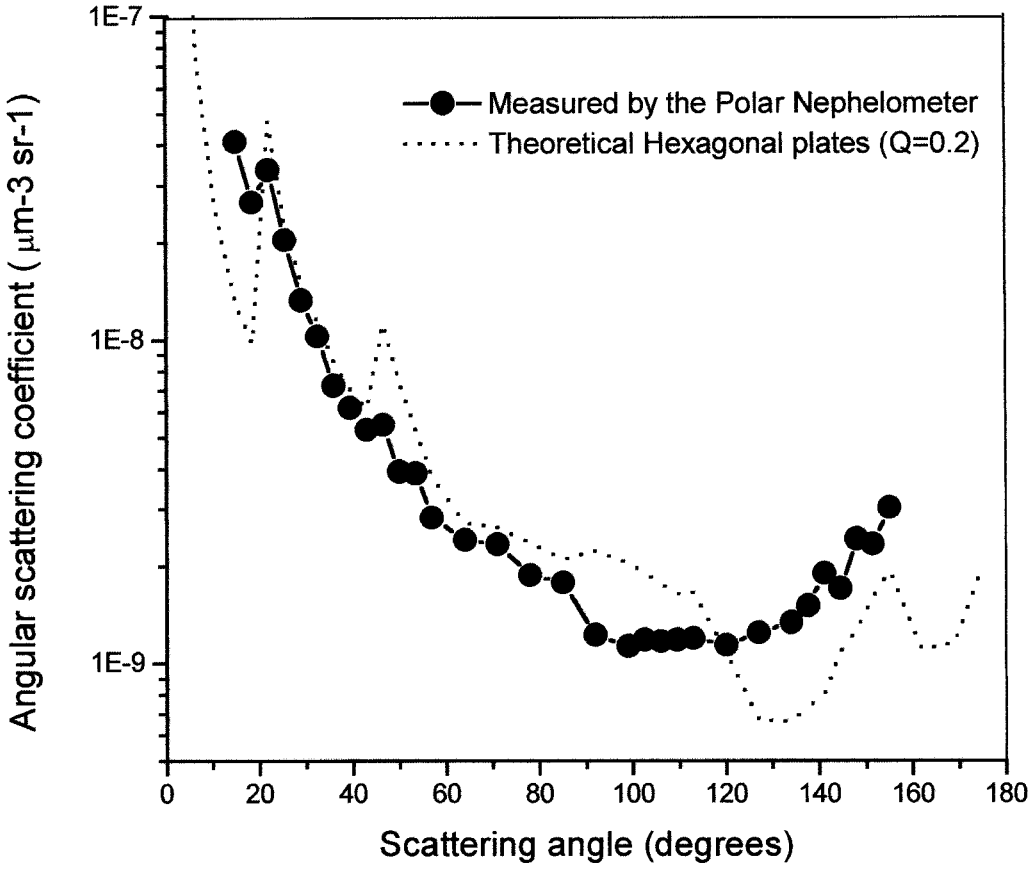

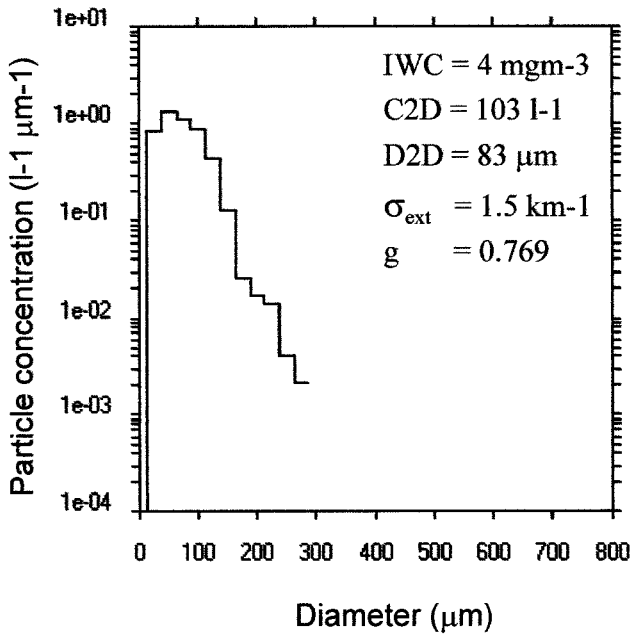

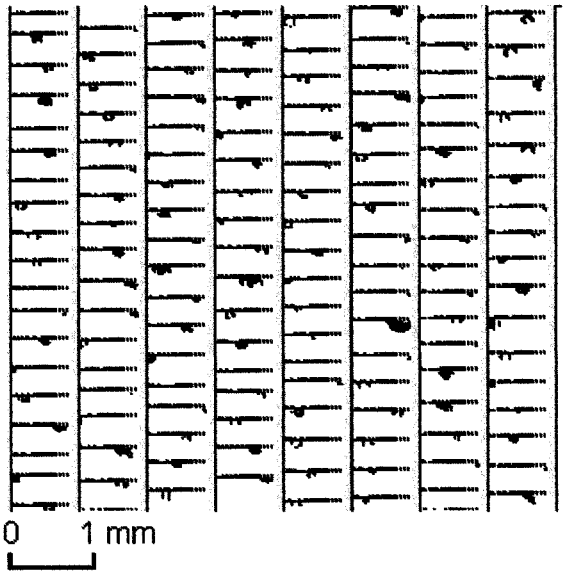

features retrieved are stronger than the instrument's signal/noise ratio and therefore are not artifacts (due to optional or electronic noise problems, for instance). Nevertheless, the examination of the measured scattering phase function in Fig. 4 reveals that the 22° and 46° peaks are rather smoothed when compared with the theoretical approach. This characteristic is systematically evidenced for all the observations reported here and will be discussed in detail in section 4c(2).

Coming back to the microphysical and optical properties of the cirrus cloud exemplified in Fig. 4, we report that the subsequent mean values of IWC, C2D, D2D, σ_{ext}, and g are 4 mg m^{-3}, 103 L^{-1}, 83 μm, 1.5 km^{-1}, and 0.769, respectively. The examination of the corresponding 2D-C probe information shows that the particle size does not exceed 300 μm with rather irregular shape at least for the largest ice crystals from which the shape recognition is less problematic. A careful examination may suggest that only a few of the largest ice crystals may be shaped as 3D assemblage like bullet-rosette type. Furthermore, some of the other recognizable ice crystals appear to be transparent because the image is blurred, but this feature could also be due to particles passing out of the depth of field (Joe and List 1987). Despite the qualitative information issued from the 2D-C probe measurement, one may conclude that ice crystals with simple geometric shape, at least larger than 100 μm, are not prevailing within this sample of ice particles.

A similar halo feature is observed during a 5-s cloud sampling from 1532:52 (see label time sequence 2 in Figs. 3 and 5 with the same representation as Fig. 4) where the microphysical and optical charateristics are noticeably different from those of the previous example. The ice water content is 6 mg m^{-3} and the extinction coefficient is twice the value reported in Fig. 4 (3.1 km^{-1} vs 1.5 km^{-1}). Subsequently, the particles are larger (D2D = 102 μm against 83 μm), as well illustrated from the 2D-C images. Clearly displayed in this example, most of the recognizable ice particles exhibit irregular shapes with sizes that do not exceed 400 μm. Nevertheless, the 22° halo is well evidenced (P7:P51 $\approx$ 1.4), whereas the 46° peak is less pronounced (P47:P10 $\approx$ 0.8).

Contrasting with this last example, the cirrus cloud sampled 5 min later at 1537:09, still at the same level (−35°C; see label 3 in Fig. 3), does not exhibit 22° and 46° halos, as clearly highlighted in Fig. 6, despite very similar microphysical and optical properties to those reported in Fig. 5. As already pointed out, the 2D-C particle images can only be considered as qualitative information, but a careful comparison between the 2D-C images in Figs. 5 and 6 suggests that no significant difference can objectively be found between the observed shapes of ice crystals.

4. Discussion

a. Horizontal heterogeneities and vertical profiles

Results in Fig. 3 reveal that at a constant flight level (−35°C), some of the cirrus uncinus cloud regions do exhibit halo features while other cloud regions are observed without any halo signature. These cloud regions are characterized by similar horizontal scale (5–10 km long) and microphysical properties (at least for those determined from the 2D-C measurements). Examination of Fig. 3 also shows that in the halo-producing cloud regions, the P7:P51 ratio is characterized by small-scale and large-amplitude fluctuations. Considering that a P7:P51 ratio larger than 1 may characterize the 22° halo occurrence, then only 2% of the cirrus do present the halo features with an horizontal scale ranging between 100 and 400 m. Notice the above observations are similar for the 46° halos.

Figures 7a–f display a composite representation (vertical profiles) of pertinent microphysical and optical parameters obtained during the ascent–descent flight sequences by the TBM700 in the cirrus layer between 1440 and 1710. It should be noticed that the values of the cloud parameters shown in Fig. 7 must only be considered as estimates because of the natural cloud inhomogeneities, the cloud time variability, and the different geographical locations of the aircraft during the corresponding flight sequences. Nevertheless, the results display a common feature of cirrus properties (see Heymsfield 1993), namely, a decrease with the temperature of the ice water content, the mean diameter, and the extinction coefficient. Due to large fluctuations of σ_{ext}, the subsequent cirrus optical depth (τ) is difficult to derive but a rough estimate gives a range between 2 and 4.

A noteworthy observation concerns the 22° halos (P7:P51 ratio >1; see Fig. 7f) that only occur near the lower cloud levels between −30° and −38°C. At higher levels no halos are evidenced even near the cloud top as illustrated on Fig. 8 (with the same representation as Fig. 4), which represents the scattering phase function and 2D-C measurements obtained at the −60°C level during 6 s from 1426:56. This figure clearly shows a smooth phase function with a value of the asymmetry factor of 0.768, and microphysical properties characterized by a

←

FIG. 4. (upper) Mean scattering phase function measured by the Polar Nephelometer (solid circles) with a typical example of theoretical scattering phase function (dotted line) relative to hexagonal crystal plates ramdomly oriented with an aspect ratio (Q) of 0.2; (lower left) corresponding 2D-C size histogram with the subsequent mean values of the relevant parameters; (Lower right) examples of ice particle images sampled by the 2D-C. Example relative to cirrus uncinus sampled at 7600 m MSL/−35°C between 1530:56 and 1531:02.

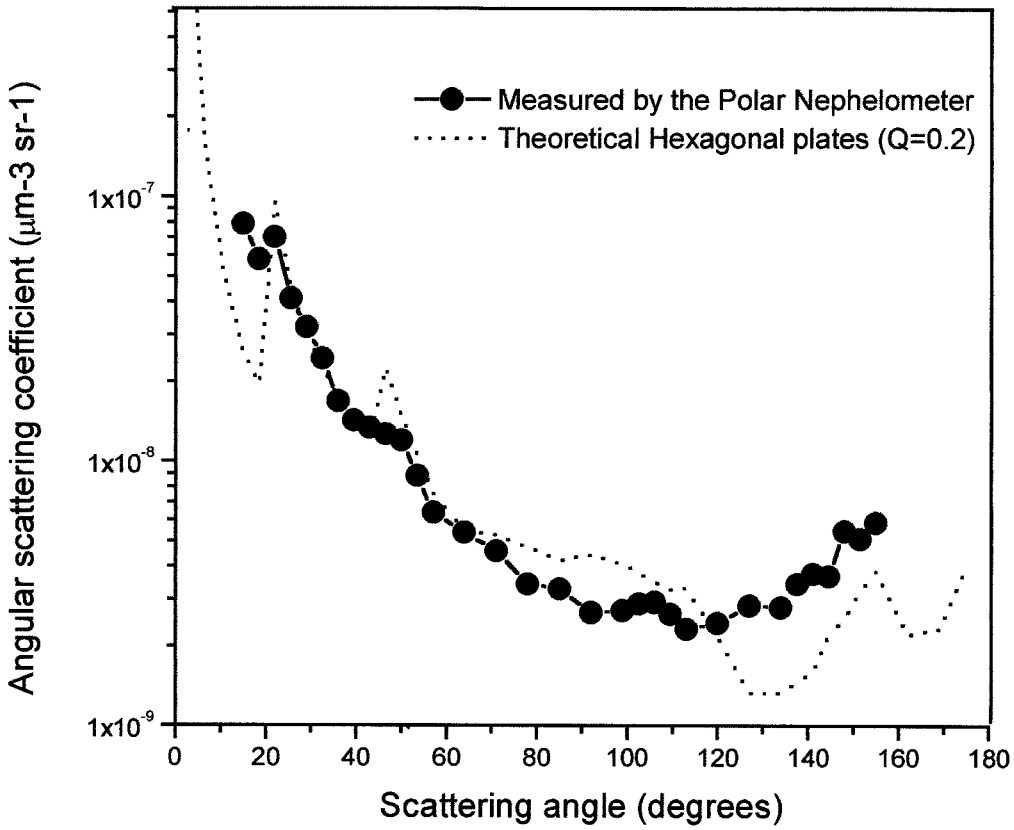

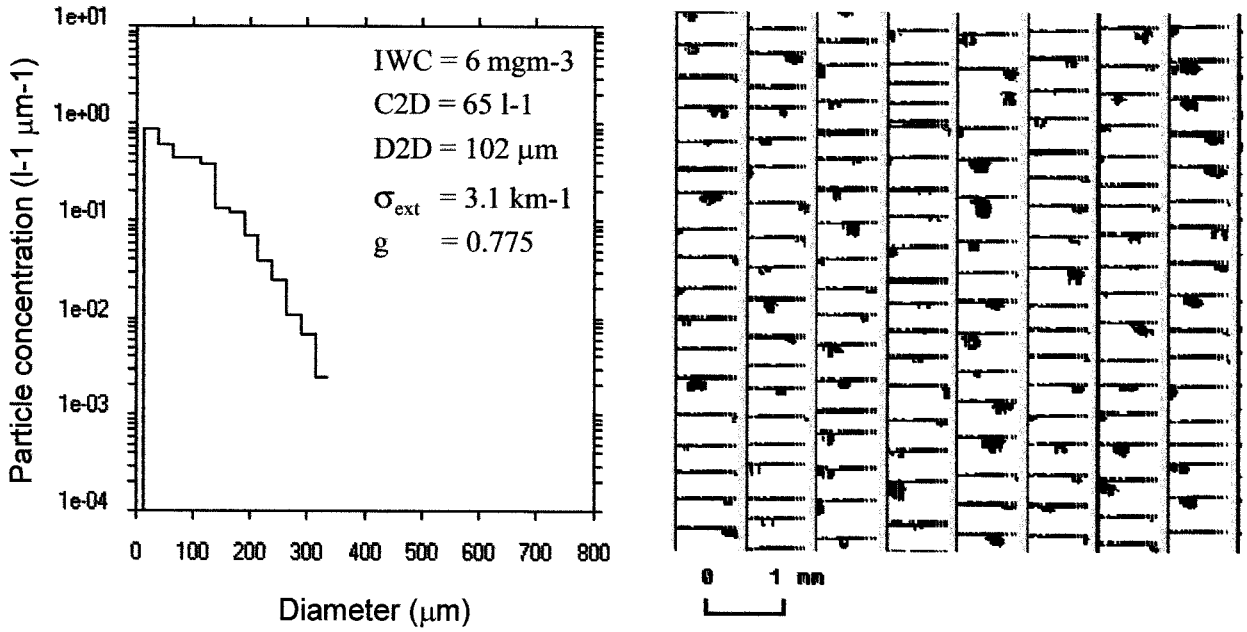

FIG. 5. Same as Fig. 4, except relative to cirrus sampled between 1532:52 and 1532:57 (7600 m MSL/−35°C).

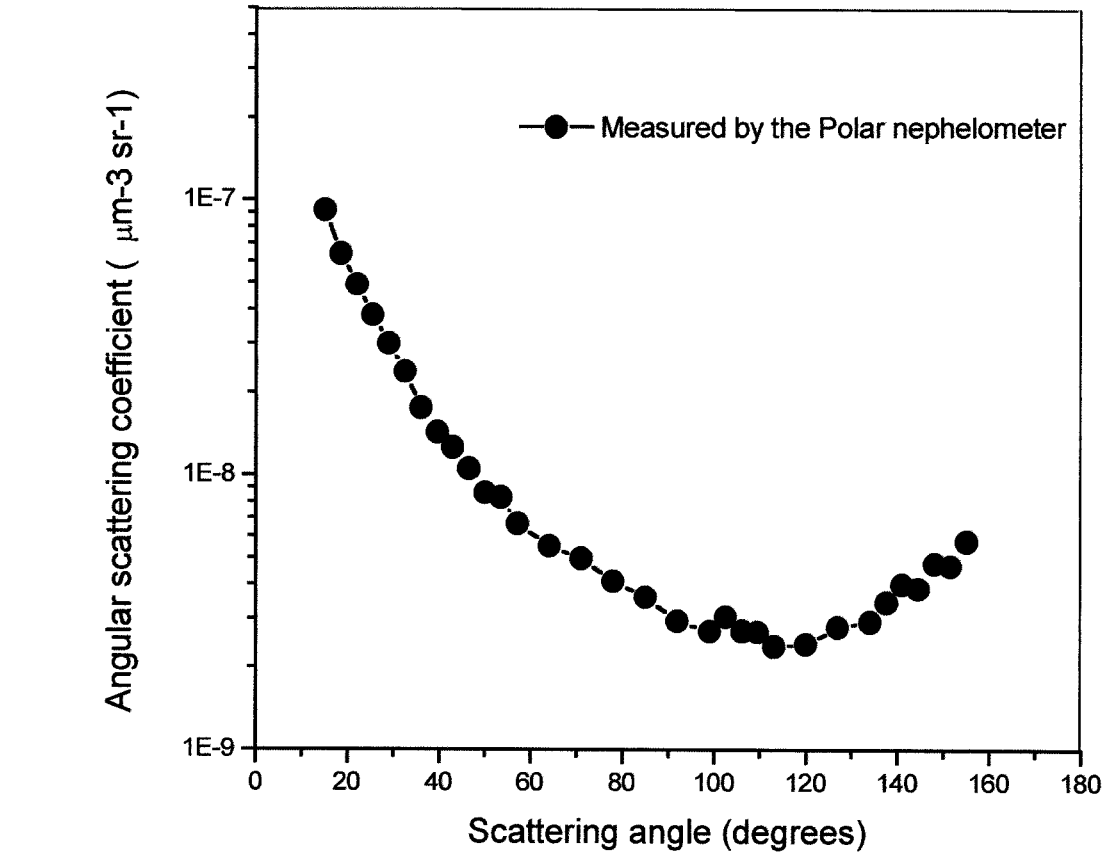

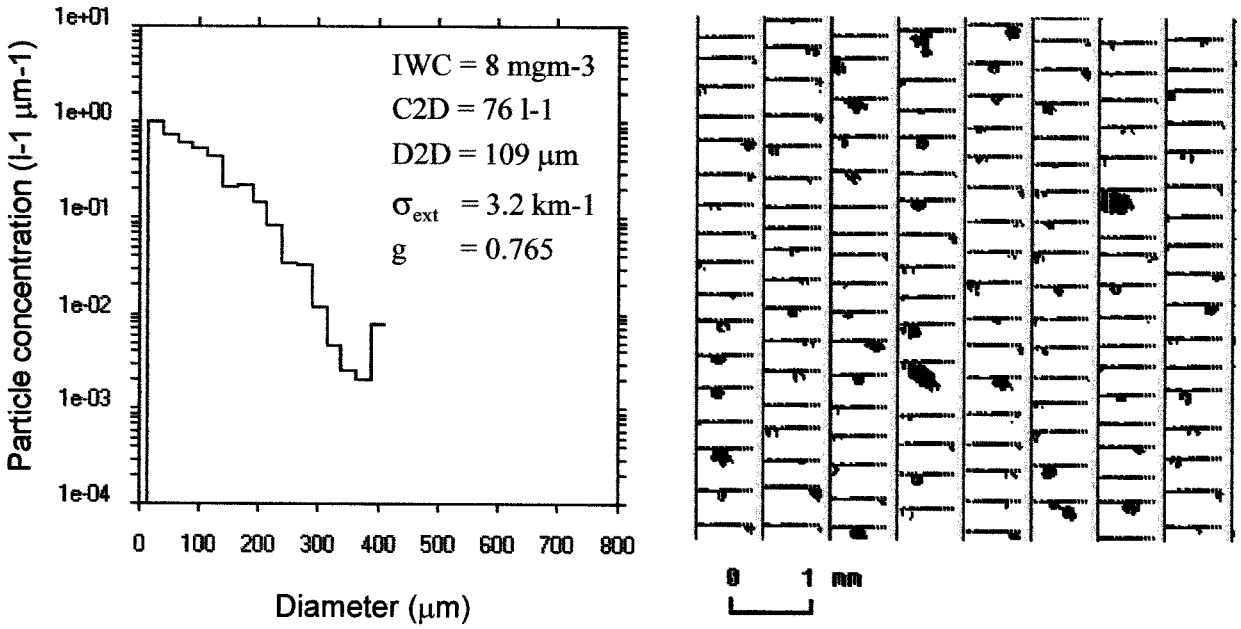

FIG. 6. Same as Fig. 4, except relative to cirrus sampled between 1537:09 and 1537:16 (7600 m MSL/−35°C).

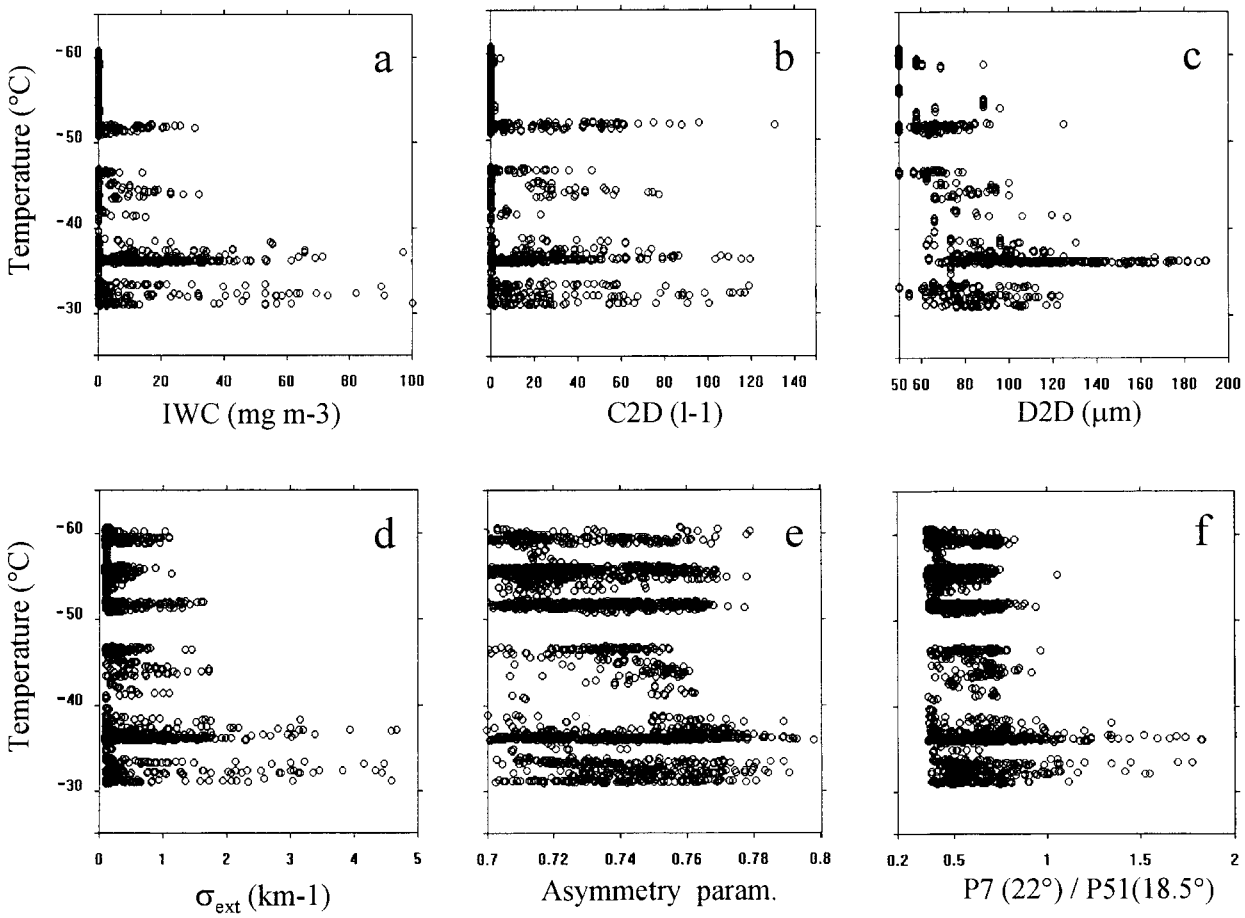

FIG. 7. Vertical profiles of cirrus uncinus microphysical and optical parameters: (a) IWC, (b) 2D-C ice particle concentration, (c) 2D-C mean diameter, (d) extinction coefficient, (e) asymmetry parameter, and (f) P7:P51 ratio.

low concentration (1 L^{-1}) of very small ice crystals (60 μm; see 2D-C images) and an extinction coefficient of only 0.7 km^{-1}.

b. Why do cirrus uncinus display halos?

The observed halo phenomena are examples of the azimuthal variability of the scattering behavior in affecting the asymmetry parameter as exemplified on Fig. 9a. The halo occurrences (P7:P51 $>$ 1) lead to larger values of the asymmetry parameter simply because the energy is more scattered in the forward direction. The corresponding g values range from 0.775 to 0.790 whereas for nonhalo occurences they are mainly between 0.735 and 0.775.

Generally, the occurrence of halo phenomena results from the simplest crystal shape (hexagonal plates and columns) and the most regular crystal shape [bullet rosettes, for instance; see, among others, Sussmann (1997)]. This criterion is not confirmed with our observations because the examination of the 2D-C images revealed that most of the ice crystals (larger than 100 μm) are irregular shaped. In a more general way we may conclude that the halo occurrences are neither related to the 2D-C particle concentration (Fig. 9b) nor to the 2D-C mean particle size larger than 50 μm (Fig. 9c).

These above observations strongly suggest that the dominant ice particles with regard to scattering properties are the small ones (typically $<$ 100 μm), which cannot quantitatively be measured by the 2D-C probe. Evidence of these small particles in cirrus clouds is now well recognized [see, among others, Platt et al. (1989); Heymsfield et al. (1990); Gayet et al. (1996b)] and the lack of accurate measurements of such ice crystals crucially limits the interpretation of our results. The above hypothesis is supported by the results in Fig. 10, which represents the extinction coefficient calculated for particles larger than 100-μm diameter (from 2D-C measurements) versus the extinction coefficient derived from the Polar Nephelometer (which measures particles larger than a few micrometers). The results show that the extinction coefficient, and therefore the cirrus cloud scattering properties, including the halo feature, are dominated ($\approx$80%) by the contribution of the particles smaller than 100 μm. Considering earlier laboratory

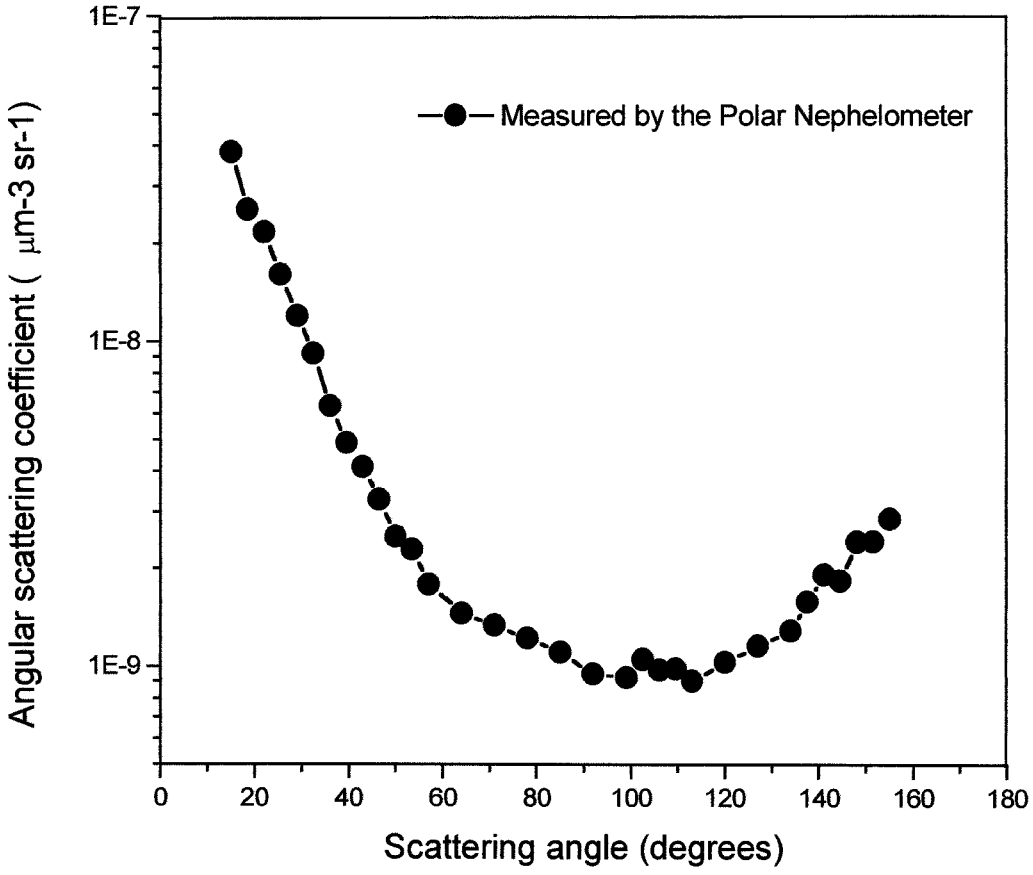

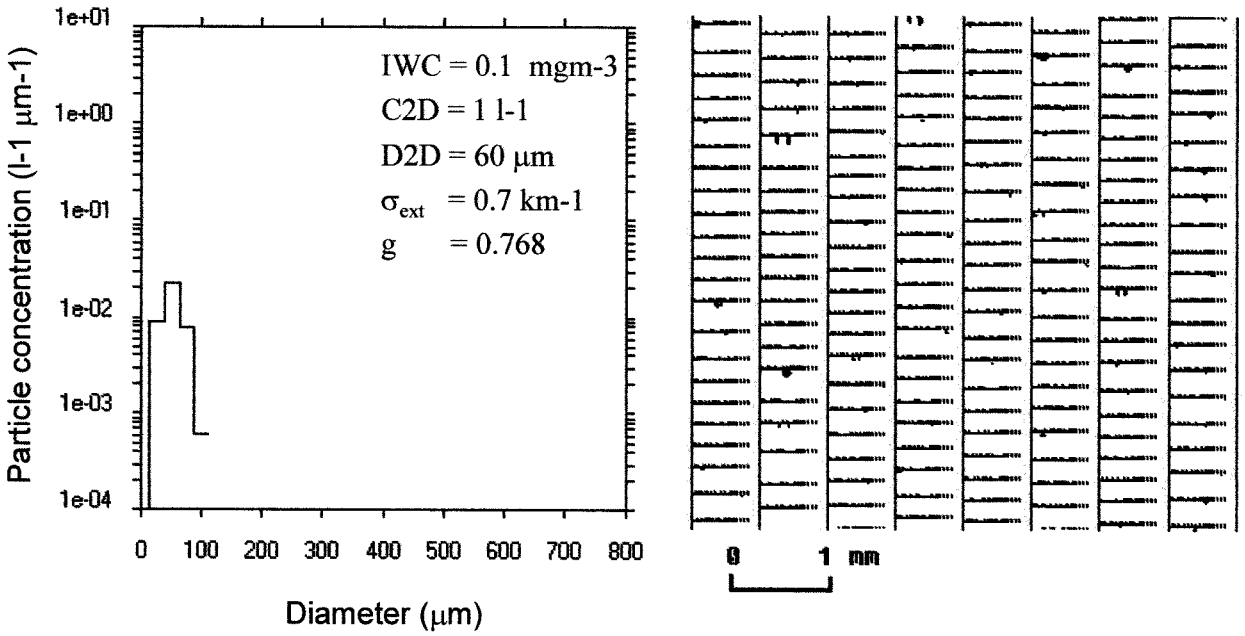

FIG. 8. Same as Fig. 4, except measurements performed between 1426:56 and 1527:03 near the cirrus cloud top (10 800 m MSL/−60°C).

studies (Sassen and Liou 1979) and recent theoretical results (Yang and Liou 1996; Mishchenko and Macke 1999) that showed that ice crystal dimensions on the order of 20 μm appear to delineate the lower limit of ice crystal size responsible for halo formation, we may suggest that crystals with size ranging on rather limited dimensions (from about 20 to 100 μm) could produce the observed halo feature. This may explain why former works [see, for instance, Glass and Varley (1978)] did not observe pristine crystal forms (in cirrus clouds) required by theory to explain optical phenomena simply because they did not use appropriate in situ instrumentation to measure the smallest ice particles.

For the highly regular crystals responsible for halo phenomena there must be a subsequent main phase of extremely regular crystal growth. Low ice supersaturations are known to favor regular and slow crystal growth (Heymsfield 1986; Pruppacher and Klett 1997) that may be found in low updraft velocities. Accordingly, and as noticed above, only a few cloud portions characterized by small horizontal scales (100–400 m) present relevant thermodynamical and dynamical conditions that may characterize formation areas of fresh ice particles. Following our observations, these areas would represent only 2% of the sampled cirrus. In addition, the low ice supersaturation condition is qualitatively supported by the fact that the halo occurrences (see Fig. 7f) are only observed in lower cirrus layer roughly ranging from -30°C to -40°C where the relative humidity is significantly lower than those measured in the upper levels as revealed by the vertical sounding in Fig. 2. At upper levels, high humidities are measured up to the cloud top (-60°C), suggesting high ice supersaturations. Most of the large (up to 400 μm) irregular-shaped ice particles observed near the cirrus base may have originated at uppermost supersaturated layers, then have grown during their fall mixing with small slow-growing pristine ice crystals. Such multilayer clouds with cirrus uncinus cells at lower levels have already been reported by Sassen et al. (1995).

Obviously a much more convincing interpretation of optical phenomenon occurrences in cirrus clouds would need additional pertinent measurements, namely, the shape and size of the small ice crystals with new advanced imager probe, like the CPI probe (Lawson 1998); the accurate and finescale structure of the low water vapor content with a cryogenic frost-point hygrometer (Ovarlez et al. 2000); the finescale structure of the dynamical parameters [wind vector and turbulence; Quante et al. (1996)] and vertical profiles of cirrus properties, which can be obtained from Lidar measurements [see, among others, Freudenthaler et al. (1994)].

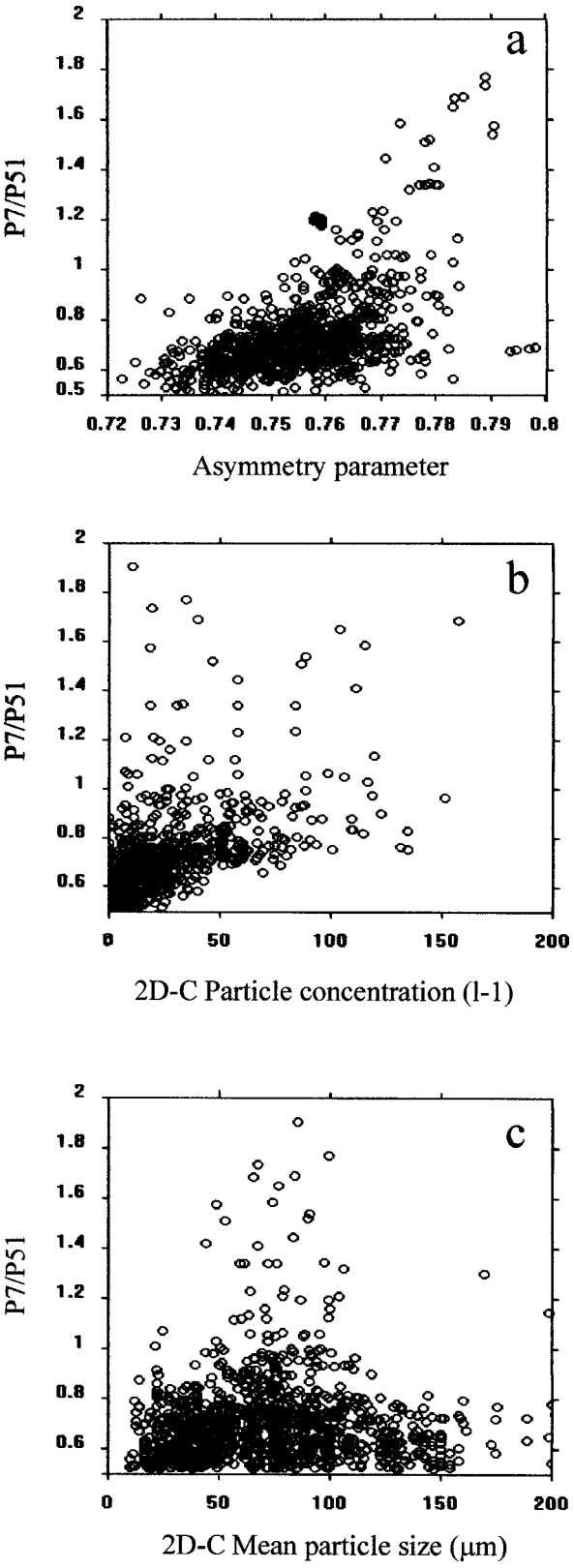

→

FIG. 9. Scatterplot measurements of P7(22°) to P51(18.5°) ratio as a function of (a) the asymmetry factor, (b) the 2D-C particle concentration, and (c) the 2D-C mean particle size.

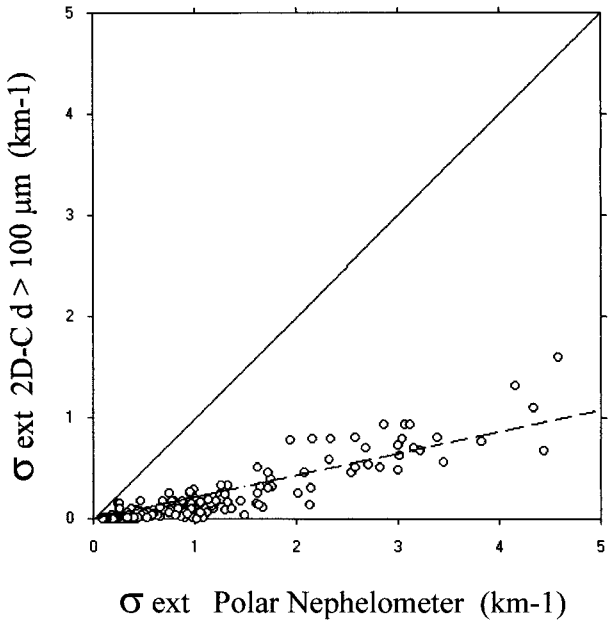

FIG. 10. Extinction coefficient calculated for particle larger than 100-μm diameter (from 2D-C measurements) vs the extinction coefficient derived from the Polar Nephelometer. Data relative to cirrus uncinus sampled at 7600 m MSL/−35°C.

c. *Why are the observed 22° and 46° halos smoothed?*

1) PROBE SHORTCOMINGS

The first hypothesis that may be addressed about the observed smoothed peaks with regard to the theory concerns the electronical bandwidth shortcomings when the Polar Nephelometer is used on aircraft. This problem has been considered during the design of the airborne version of the probe. Laboratory tests (Jourlin 1997) showed that the upper limits of the electronical bandwidth of each channel (or measured scattering angle) were compatible with an airspeed of up to 200 m s^{-1}. This was confirmed from airborne measurements of the scattering phase function in water stratiform clouds, which highlighted a very good agreement when compared with the derived phase function from direct measurements of the droplet size distribution (Gayet et al. 2000).

The second hypothesis may be the aerodynamic flow effects on crystal orientation caused by the probe inlet ahead of the sampling section. This problem was carefully considered with PMS probes by McPherson and Baumgardner (1988). In our case, 2D numerical simulations have been performed in order to determine the stream flow around and inside both the probe inlet and the sampling section (Soulhac 1996), but nothing is known about the flow effect perturbation on the Polar Nephelometer response in the presence of oriented ice crystals. Nevertheless, we may point out that plate-shaped particles tend to fall oriented (Ono 1969) only for Reynolds numbers between 1 and 100 (Sassen 1980), that is, for crystal sizes ranging from 300 μm to 2 mm. Considering that the measured cirrus uncinus ice particles are much smaller than 400 μm, they will tend to fall randomly oriented even if they are plate shaped. We may consider in this case that the hypothetical flow effects might not disturb the scattering phase function measurements. This conclusion is supported by results that evidenced smoothed 22° peaks from quasi-static tests (with probable small flow perturbation) in a cold chamber where hexagonal ice crystals were produced from AgI seeding (Crépel et al. 1997).

Consequently the above arguments suggest that the smoothed 22° and 46° peaks are not artifacts due to probe shortcomings but can be regarded as a physical phenomenon. We will now discuss results of numerical simulation of light scattering in order to interpret these observed optical characteristics.

2) MODELING OF LIGHT SCATTERING BY CIRRUS CLOUD PARTICLES

The Inhomogeneous Hexagonal Monocrystal (IHM) model has been used to simulate light scattering by randomly oriented hexagonal ice crystals containing air bubbles. Doutriaux-Boucher et al. (2000) and Labonnote et al. (2000) clearly demonstrated the reliability of the IHM model for the simulation of the radiative properties of ice clouds as well as in terms of spherical albedo than in terms of polarized radiances. For instance, better results are obtained than in the polycrystal model in terms of radiatively equivalent particles in order to retrieve radiative properties of ice clouds (Labonnote et al. 2001).

This model being thoroughly described in a previous paper (Labonnote et al. 2001), we recall here that the ice crystals are defined by their aspect ratio (Q), the diameter of a volume equivalent spherical particle (Dv), and the mean free path between air bubbles (l). The air bubble size distribution follows a gamma standard law characterized by effective diameter and effective variance of 1.0 and 0.1 μm, respectively. Calculations have been made at $\lambda = 804$ nm in order to compare the results with the Polar Nephelometer measurements.

Two populations of ice particles have been considered. According to the 2D-C measurements, the first population considers large irregular-shaped particles characterized by a volume equivalent spherical diameter of 50 μm. This value roughly corresponds to the measured particle mean size (*D2D* ranges from 83 to 102 μm; see Figs. 4 and 5) by considering the mass–size relationship used in the method of 2D-C data processing (Gayet et al. 1996a). The irregular shape of the particles is represented by an aspect ratio (Q) of 1.0, and a relative small value of the mean free path (i.e., $l = 10$ μm) has been set in order to simulate a rather inhomogeneous particle. The results of the simulation reported in Fig. 11 show that the 22° and 46° peak features are smoothed

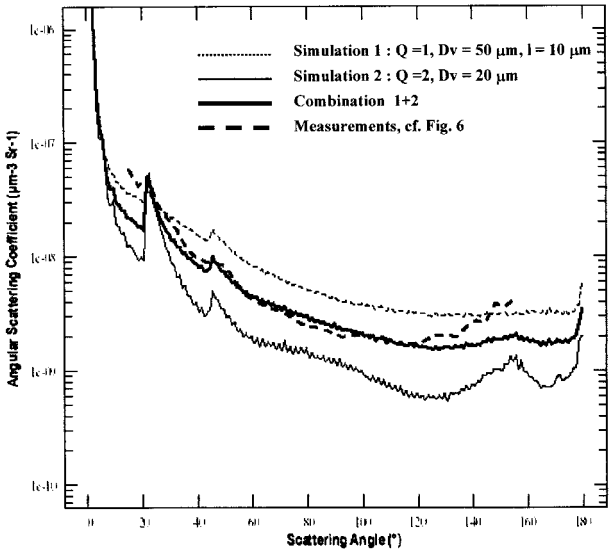

FIG. 11. Comparison between in situ measurements (see Fig. 6) and IHM scattering phase functions.

out when inhomogeneous particles are considered (i.e., by incorporating air bubble inclusions in the calculations).

The second ice particle population hypothecizes small pristine ice crystals. Owing to a temperature around −35°C, particle column shape with an aspect ratio of 2.0 is assumed. Without quantitative information about the size of ice particles smaller than 25 μm, an equivalent diameter of 20 μm has been assumed in the IHM model. This value corresponds to the lower limit of the size parameter for which the ray-tracing technique (at visible wavelengths) can produce well-defined 22° and 46° halos (see Mishchenko and Make 1999). The results of this simulation are superimposed on Fig. 11 and the resultant scattering phase function has been calculated using a mixture of the two ice populations. In order to match the results with the measurements reported in Fig. 5, the concentration of large particles has been set to 65 L^{-1} (C2D) and the small pristine ice crystals concentration has been tuned to 385 L^{-1}, leading to a total particle concentration of 450 L^{-1}.

The results in Fig. 11 show that the modeled results fit with a rather good agreement the measurements of the scattering phase function measured by the Polar Nephelometer, particularly near the halo region. The combination of two populations of ice particles may therefore explain the observed smoothed-peaks feature of the measured scattering phase function. On the contrary, the IHM results do not match very well the measurements at both forward and backward directions. However, we cannot exclude other possibilities of the microphysical model since a smooth phase function can also be obtained from inclusions in crystals with different shapes and/or irregularities at the crystal surface (Liou et al. 1998). The smoothed-peaks behavior may also be explained by a mixed population of small ice particles (i.e., <20 μm, see Oshchepkov et al. 2000) that do not generate halos and larger pristine ice crystals. Appropriate measurements of small ice crystal properties would be of a prime interest in order to investigate the reliably of ice crystal models.

5. Conclusions

Using the Polar Nephelometer, a new instrument for in situ measuring of the scattering phase function of cloud droplets and ice particles, 22° and 46° halo features have been evidenced during a cirrus uncinus cloud case study between −30°C and −38°C. Simultaneous microphysical measurements were made with the PMS 2D-C probe. In halo-producing cirrus clouds, most of the ice crystals larger than 100 μm were observed with irregular shapes and no significant difference in the shape of ice crystals has been objectively found between the cirrus parts with and without halo. More generally, halo occurrences were not related to the ice particle properties derived from the 2D-C probe. Therefore, we obtained proof that the cloud scattering properties and the subsequent optical phenomena are dominated by the smallest ice particles (smaller than 100 μm), which are poorly documented with conventional PMS probes. This may explain why former works did not relate pristine crystal forms (in cirrus clouds) required by theory to explain optical phenomena simply because they did not use appropriate in situ instrumentation to measure small ice particles. Hypothesizing that highly regular small crystals are responsible for halo phenomena, there must be a subsequent main phase of extremely regular crystal slow growth that requires low ice supersaturation. Only a few cirrus cloud portions that are characterized by small horizontal scales (100–400 m) did present such relevant thermodynamical and dynamical conditions, which may characterize formation areas of fresh ice particles. Following our observations, these areas would represent a proportion of only 2% of the sampled cirrus. Moreover, the observed 22° and 46° smoothed-peak features may be explained by the results of the Inhomogeneous Hexagonal Monocrystal (IHM) model of light scattering considering the combination of two populations (large irregular and small pristine) of ice particles.

Because these results relate only to a case study with rather limited instrumentation, a more convincing interpretation of optical phenomena occurrences in cirrus clouds would need additional pertinent measurements, namely, the shape and the size of the small ice crystals, the accurate and finescale structure of both the low water vapour content and the dynamical parameters (wind and turbulence), and the vertical profiles of the cirrus optical properties (lidar measurements).

Acknowledgments. This work was supported by the French Direction des Systèmes de Forces et de la Prospective/Service Technique des Technologies Com-

munes within the ONERA contract n° 23.140/DA.B1/BC. We are very grateful to J.-F. Fournol and O. Crépel for their active participation in the experiment. The authors would like to give recognition to G. Durand (ONERA) for his kind help in aircraft data processing. Thanks are extended to A.-M. Lanquette (LaMP) for her cooperation in the weather analysis. We also thank the members of SOCATA in Tarbes who operated the TBM700 aircraft during the experiment. We are grateful to anonymous reviewers for their helpful comments.

REFERENCES

Auriol, F., 1998: Mesure in situ de la fonction de phase de diffusion des particules nuageuses au moyen du Néphélomètre Polaire aéroporté: Validation et application aux nuages glacés. Ph.D. thesis, *Université Blaise Pascal,* 151 pp.

Brogniez, G., J. C. Buriez, V. Giraud, F. Parol, and C. Vanbauce, 1995: Determination of effective emittance and aradiatively equivalent microphysical model of cirrus from ground-based and satellite observations during the International Cirrus Experiment: The 18 October 1989 case study. *Mon. Wea. Rev.,* **123,** 1025–1036.

Crépel, O., J.-F. Gayet, J.-F. Fournol, and S. Oshehepkov, 1997: A new airborne Polar Nephelometer for the measurements of optical and microphysical cloud properties. Part II: Preliminary tests. *Ann. Geophys.* **15,** 460–470.

Doutriaux-Boucher, M., J.-C. Buriez, G. Brogniez, L.-C. Labonnote, and A. J. Baran, 2000: Sensitivity of retrieved POLDER directional cloud optical thickness to various ice particles models. *Geophys. Res. Lett.,* **27** (1), 109–112.

Durand G., J.-F. Gayet, L. Kaës, and P. Matharan, 1998: Airborne infra red and microphysical measurements in cirrus clouds. *Satellite Remote Sensing of Clouds and Atmosphere III,* J. E. Russel, Ed., Vol. 3495, *Proc. SPIE,* 72–81.

Eide, H. A., J. J. Stamnes, K. Stamnes, and F. M. Schulz, 1999: New method for computing expansion coefficients for spheroidal functions. *J. Quant. Spectrosc. Radiat. Trans.,* **63,** 191–203.

Francis, P. N., 1995: Some aircraft observations of the scattering properties of ice crystals. *J. Atmos. Sci.,* **52,** 1142–1154.

Freudenthaler, V., F. Homburg, and H. Jäger, 1994: Ground-based Contrail mobile scanning LIDAR for remote sensing of contrails. *Ann. Geophys.,* **12,** 956–961.

Gayet, J.-F., G. Febvre, G. Brogniez, H. Chepfer, W. Renger, and P. Wendling, 1996a: Microphysical and optical properties of cirrus and contrails: Cloud field study on 13 October 1989. *J. Atmos. Sci.,* **53,** 126–138.

——, ——, and H. Larsen, 1996b: On the reliability of the PMS FSSP probe in the presence of small ice crystals. *J. Atmos. Oceanic Technol.,* **13,** 1300–1310.

——, O. Crépel, J.-F. Fournol, and S. Oshchepkov, 1997: A new airborne Polar Nephelometer for the measurements of optical and microphysical cloud properties. Part I: Theoretical design. *Ann. Geophys.,* **15,** 451–459.

——, and Coauthors, 1998: In situ measurements of the scattering phase function of stratocumulus, contrails and cirrus. *Geophys. Res. Lett.,* **25,** 971–974.

——, S. Asano, A. Yamazaki, A. Uchiyama, A. Sinyuk, F. Auriol, and O. Jourdan, 2000: Microphysical and optical properties of winter boundary layer clouds over the sea: Two case studies of continental-type water and maritime mixed-phased stratocumuli. *Proc. Int. Conf. on Clouds and Precipitation,* Reno, NV, ICCP/IAMAS, 744–747.

Gerber, H., Y. Takano, T. J. Garrett, and P. V. Hobbs, 2000: Nephelometer measurements of the asymmetry parameter, volume extinction coefficient, and backscatter ratio in arctic clouds. *J. Atmos. Sci.,* **57,** 3021–3034.

Glass, M., and D. J. Varley, 1978: Observations of cirrus particle characteristics occurring with halos. Preprints, *Conference on Cloud Physics and Atmospheric Electricity,* WA, Amer. Meteor. Soc., 126–128.

Heymsfield, A. J., 1986: Ice particles observed in a cirriform cloud at −83°C and implications for polar stratospheric clouds. *J. Atmos. Sci.,* **43,** 851–855.

——, 1993: Microphysical structures of stratiform and cirrus clouds. *Aerosol–Cloud–Climate Interactions,* P. V. Hobbs, Ed., Academic Press, 97–121.

——, K. Miller, and J. D. Spinhirne, 1990: The 27–28 October 1986 FIRE IFO cirrus case study: Cloud microstructure. *Mon. Wea. Rev.,* **118,** 2313–2328.

Joe, P., and R. List, 1987: Testing and performance of two-dimensional optical array spectrometers with greyscale. *J. Atmos. Oceanic Technol.,* **4,** 139–150.

Jourlin, Y., 1997: Qualification aéroportée du Néphélomètre Polaire. Tech. Rep. LaMP, Université Blaise Pascal, Clermont-Ferrand France, 113 pp. [Available from LaMP, Université Blaise Pascal, 24 av. des Landais, 63177 Aubiére France.]

Knap, W. H., M. Hess, P. Stammes, R. B. A. Koelemeijer, and P. D. Watts, 1999: Cirrus optical thickness and crystal size retrieval from ATSR-2 data using phase functions of imperfect hexagonal ice crystals. *J. Geophys. Res.,* **104,** 31 721–31 730.

Korolev, A. V., G. A. Isaac, and J. Hallett, 1999: Ice particle habits in Arctic clouds. *Geophys. Res. Lett.,* **26,** 1299–1302.

Labonnote, L. C., G. Brogniez, J.-F. Gayet, M. Doutriaux-Boucher, and J. Buriez, 2000: Modeling of light scattering in cirrus clouds with inhomogeneous hexagonal monocrystals. Comparison with in situ and ADEOS-POLDER measurements. *Geophys. Res. Lett.,* **27,** 113–116.

——, J.-C. Buriez, M. Doutriaux-Boucher, J.-F. Gayet, and A. Macke, 2001: Polarized light scattering by inhomogeneous hexagonal monocristals. Validation with ADEOS-POLDER measurements. *J. Geophys. Res.,* **106,** 12 139–12 153.

Larsen, H. R., J.-F. Gayet, G. Febvre, H. Chepfer, and G. Brogniez, 1998: Measurement errors in cirrus cloud microphysical properties. *Ann. Geophys.,* **16,** 266–276.

Lawson, R. P., 1998: A comparison of ice crystal observations using a new cloud particle imaging probe in Arctic cirrus and a decaying anvil in Texas. *Opt. Soc. Amer. Tech. Digest,* 113–115.

——, and T. L. Jensen, 1998: Improved microphysical observations in mixed phase clouds. Preprints, *Conf. on Cloud Physics,* Everett, WA, Amer. Meteor. Soc., 451–454.

Liou, K. N., P. Yang, Y. Takano, K. Sassen, T. P. Charlock, and W. P. Arnott, 1998: On the radiative properties of contrail cirrus. *Geophys. Res. Lett.,* **25,** 1161–1164.

——, Y. Takano, and P. Yang, 1999: Light scattering and radiative transfer in ice crystal clouds: Applications to climate research. *Light Scattering by Nonspherical Particles: Theory, Measurements and Geophysical Applications,* M. I. Mishchenko, J. W. Hovenier, and L. D. Travis, Eds., Academic Press, 417–449.

Macke, A., and M. I. Mishchenko, 1998: Monte Carlo calculations of light scattering by large particles with multiple internal inclusions. Preprints, *Conf. on Light Scattering by Nonspherical Particles: Theory, Measurements, and Applications.* New York, NY, Amer. Meteor. Soc., 143–146.

MacPherson, J. I., and D. Baumgardner, 1988: Airflow about King Air wingtip-mounted cloud particle measurement probes. *J. Atmos. Oceanic Technol.,* **5,** 259–273.

Mariotte, E., 1717: Œuvres de Mr. Mariotte. *Traité des couleurs,* Vol. 1, P. Vander, Ed., 272–281.

Mishchenko, M. I., and A. Macke, 1999: How big should hexagonal ice crystals be to produce halos? *Appl. Opt.,* **38,** 1626–1629.

Ono, A., 1969: The shape and riming properties of ice crystals in natural clouds. *J. Atmos. Sci.,* **26,** 138–147.

Oshchepkov, S. L., O. V. Dubovik, and T. V. Lapyonok, 1993: A method of numerical solution of line-inverse problem with log-normal noise distribution: The estimation of aerosol size distribution. *IRS-92 Current Problems in Atmospheric Radiation.* S. Keevallik and O. Kärner, Eds., A. Deepak, 334–337.

——, H. Isaka, J.-F. Gayet, A. Sinyuk, F. Auriol, and S. Havemann, 2000: Microphysical properties of mixed-phase and ice clouds retrieved from in situ airborne Polar Nephelometer measurements. *Geophys. Res. Lett.,* **27,** 209–213.

Ovarlez, J., P. van Velthoven, G. Sachse, S. Vay, H. Schlager, and H. Ovarlez, 2000: Comparison of water vapor measurements from POLINAT 2 with ECMWF analyses in high humidity conditions. *J. Geophys. Res.,* **105,** 3737–3744.

Platt, C. M. R., J. D. Spinhirne, and W. D. Hart, 1989: Optical and microphysical properties of a cold cirrus cloud: Evidence for regions of small ice particles. *J. Geophys. Res.,* **94,** 151–164.

Pruppacher, H. R., and J. D. Klett, 1997: *Microphysics of Clouds and Precipitation.* Kluwer Academic, 954 pp.

Quante, M., P. R. A. Brown, R. Baumann, B. Guillemet, and P. Hignett, 1996: Three-aircraft intercomparison of dynamical and thermodynamical measurements during the Pre-EUCREX campaign. *Beitr. Phys. Atmos.,* **69,** 129–146.

Sassen, K., 1980: Remote sensing of planar ice crystal fall attitudes. *J. Meteor. Soc. Japan,* **58,** 422–429.

——, and K. N. Liou, 1979: Scattering of polarized laser light by water droplets, mixed phase and ice clouds. Part I: Angular scattering patterns. *J. Atmos. Sci.,* **36,** 838–851.

——, and Coauthors, 1995: The 5–6 December 1991 FIRE IFO II jet stream cirrus case study: Possible influence of volcanic aerosols. *J. Atmos. Sci.,* **52,** 97–123.

Soulhac, L., 1996: Projet Népéhlomètre: Etude aérodynamique. Tech. Note O.P.G.C. n° 137, LaMP, Université Blaise Pascal, 79 pp. [Available from LaMP, Université Blaise Pascal, 24 av. des Landais, 63177 Aubiére France.]

Sussmann, R., 1997: Optical properties of contrail-induced cirrus: Discussion of unusual halo phenomena. *Appl. Opt.,* **36,** 4195–4201.

Takano, Y., and K. N. Liou, 1989: Solar radiative transfer in cirrus clouds. Part I: Single-scattering and optical properties of hexagonal ice crystals. *J. Atmos. Sci.,* **46,** 3–18.

——, and ——, 1995: Radiative transfer in cirrus clouds. Part III: Light scattering by irregular ice crystals. *J. Atmos. Sci.,* **52,** 818–837.

Tape, W., 1994: Atmospheric halos. *Antarctic Research Series,* Vol. 64, Amer. Geophys. Union, 143 pp.

Volkovitskiy, O. A., L. N. Pavlova, and A. G. Petrushin, 1980: Scattering of light by ice crystals. *Izv. Atmos. Ocean Phys.,* **16,** 90–102.

Yang, P., and K. N. Liou, 1996: Finite-difference time-domain method for light scattering by small ice crystals in three dimensional space. *J. Opt. Soc. Amer.,* **A13,** 2072–2085.

——, and ——, 1998: Single-scattering properties of complex ice crystals in terrestrial atmosphere. *Contrib. Atmos. Phys.,* **71,** 223–248.